IOP Conf. Series: Journal of Physics: Conf. Series **827** (2017) 012013 doi:10.1088/1742-6596/827/1/012013

Pressure-induced metallic ferromagnetism in antiferromagnetic insulator LaMnAsO

HuaiBao Tang[a,*], Guang Li[a], Qun Yang[a], XueQing Zuo[a], HaiJun Zhang[a] and DaYong Liu[b,]**

a School of Physics and Materials Science, Anhui University, Hefei 230039, China
b Key Laboratory of Materials Physics, Institute of Solid State Physics, Chinese Academy of Sciences, P. O. Box 1129, Hefei, Anhui 230031, China

E-mail: * hbtang@ahu.edu.cn, ** dyliu@theory.issp.ac.cn

Abstract. Based on the first-principles calculations, we investigate the effects of the hydrostatic pressure on the layered oxypnictide LaMnAsO, and predict that it undergoes a transition from a G-type antiferromagnetic (AFM) insulator to a ferromagnetic (FM) metal at the critical pressure $P_c \sim 18.0$ GPa, accompanied by a high-spin state with $m_{Mn} = 2.65\ \mu_B$ to a low-spin one with $m_{Mn} = 1.63\ \mu_B$ transition, or magnetic moment collapse. Our calculations identify that it is the hydrostatic pressure that collapses the G-type AFM gap, and the large density of state (DOS) around Fermi level stabilizes the FM metallic phase due to the Stoner instability. The pressure-induced AFM insulator to FM metal transition opens up the possibility of two state device applications in the oxypnictide LaMnAsO compound.

1. Introduction

Since the discovery of hight-temperature superconductivity in fluorine-doped LaFeAsO [1, 2, 3], the quaternary compounds with ZrCuSiAs-type (abbreviated as 1111-type) structure have recently attracted considerable interest as advanced electronic functional materials. With full replacement of the Fe sites by other transition metals, a larger number of layered transition metal arsenide oxide *Ln*MAsO (*Ln*: lanthanoid, *M*: transition metal) have been synthesized and studied experimentally, meanwhile they exhibit many interesting properties: besides LaFeAsO serving as mother compound for hight-temperature superconductor, they exhibit giant magnetoresistance and rare earth magnetism in *Ln*MnAsO [4, 5, 6, 7], itinerant ferromagnetism in *Ln*CoAsO [8, 9, 10, 11], low temperature superconductivity and Kondo physics in *Ln*NiAsO [12, 13, 14], and glassy magnetism in *Ln*RuAsO [15].

Of particular interest is the Mn-based 1111 material LaMnAsO, which is an in-plane AFM insulator with an experimental gap of ~ 1.1 eV [5,16]. The Mn atoms order in a checkerboard fashion termed as G-type antiferromagnetism, with the spins aligned collinear to the c axis [17]. The Néel temperature is 360 K, and the local moment at the Mn site is large, $\sim 3.34\ \mu_B$ [17], contrary to the small moment of $0.4 \sim 0.8\ \mu_B$ per Fe atom seen in the stripe-like (C-type) AFM ground state of the isostructure LaFeAsO [18]. Band structure calculations [19] indicate as well that LaMnAsO is G-type AFM despite an even smaller gap values of ~ 0.2 eV.

The AFM and insulating ground state of LaMnAsO could recall those of the parent compound of cuprate superconductors, where the highest T_c occurs when pressure or doping transform the localized electrons in the AFM insulator into itinerant carriers in the metal. With those in view,

even larger T_c may be desirable in the isostructural Mn analog of Fe-based superconductors, provided that a stabilizing metallic state is achieved. Indeed, the essentially metallic behavior was displayed in $La_{1-x}Sr_xMnAsO$ via hole doping [20], and associated with metallization via electron doping, ferromagnetism with negative magnetoresistance was also observed in $LaMnAsO_{1-x}H_x$ for $x > 0.14$ [21]. It is natural to ask whether or not the AFM insulator to FM metal transition occurs in the pressured LaMnAsO.

In this paper we present the magnetic properties of the layered manganese oxyarsenide LaMnAsO under hydrostatic pressure obtaining by the first-principles calculations. Our results clearly show that a transition from a low-pressure AFM insulator to a high-pressure bulk FM metal when the pressure is increased to the critical value $P_c \sim 18$ GPa. Such a magnetic property could be useful in two state sensor device. The rest of the paper is organized as follows: we describe the crystal structures of pressured LaMnAsO and computational method in Sec. II, and present the numerical results and discussions in Sec.III, and Sec.IV is devoted to the summary.

2. Structure and computational methods

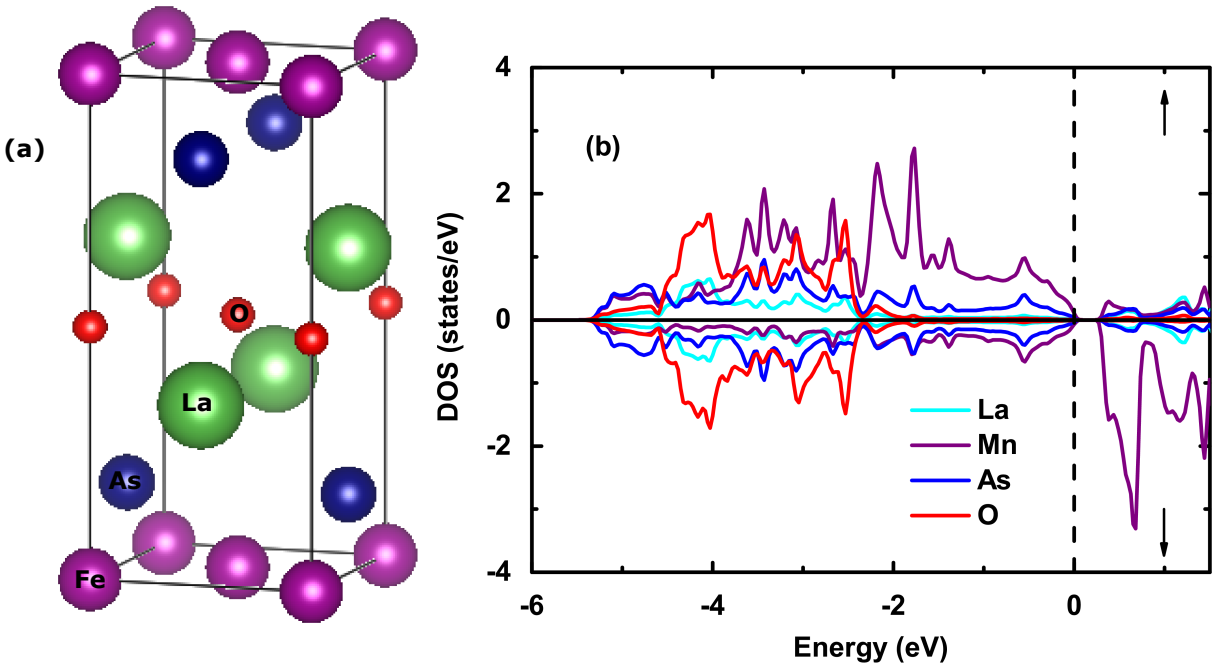

Figure 1. (Color online) (a) Unit cell of crystal structure of LaMnAsO and (b) Spin-polarized atom-projected density of states (PDOS) of the G-type AFM state in ambient pressure obtained by GGA.

As shown in Fig. 1 (a), LaMnAsO has a layered tetragonal crystal structure with the space group P4/*nmm*, where the charge donor LaO layers are sandwiched between the functional MnAs layers in an ABA sequence. In the essential MnAs layers, each Mn cation is caged by an edge-sharing As tetrahedron, defining a two-dimensional square Mn atomic lattice. To study the electronic structure and magnetic properties of LaMnAsO under the hydrostatic pressure, we have used the following structural optimization procedure: we fix the unit cell volume and optimize the c/a ratio and all internal atomic coordinates for the tetragonal lattice. Manually changing the lattice volume allows for the investigation of different hydrostatic pressure, and the Birch-Murnaghan equation of state is used to estimate the theoretical pressure.

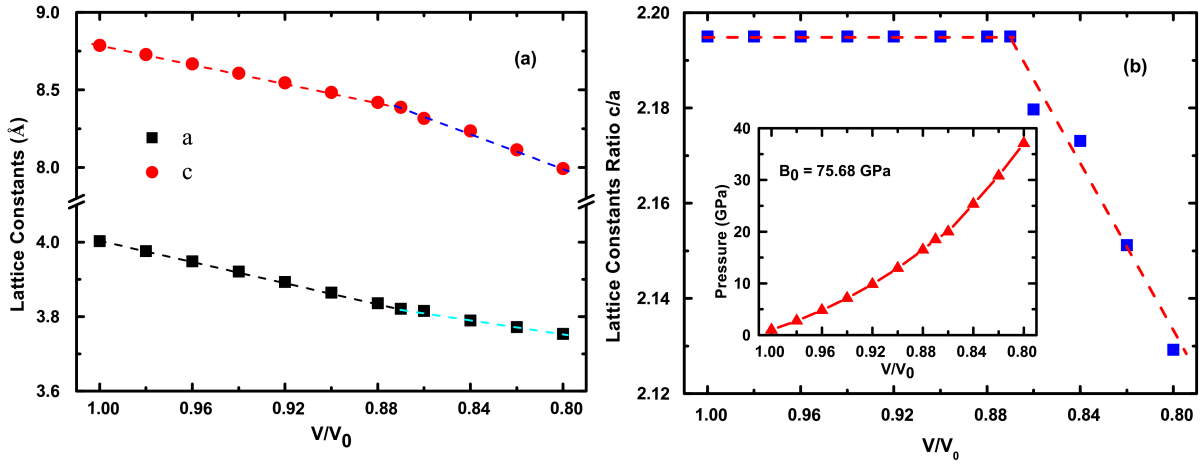

Figure 2. (Color online) (a) The tetragonal lattice cell parameters of LaMnAsO, a and c, versus unit cell volume. (b) The c/a ratio versus unit cell volume, inset: the pressure intensity versus unit cell volume with the bulk modulus B_0.

The calculations reported here are performed by using full-potential linearized augmented plane wave (FP-LAPW) method based on density functional theory (DFT), as implemented in the WIEN2k package [22]. For the exchange correlation potential, we used the generalized gradient approximation (GGA) in the Perdew-Burke-Ernzerhof variant [23]. The number of k points was 1000 for the tetragonal unit cell. The C-type AFM unit cell size is doubled to $\sqrt{2} \times \sqrt{2} \times 1$. The self-consistent calculations are considered to be converged when the total energy difference of the crystal does not exceed 0.1 mRy and that in the total electronic charge does not exceed 10^{-4} electronic charge at consecutive steps. All independent internal atomic coordinates are optimized until the corresponding forces are less than 1 mRy/$a.u.$.

3. Results and discussions

Table 1. The GGA results of LaMnAsO at ambient pressure. The NM state is the referent state for the energy.

Magnetic Order	Energy (meV/Mn)	Moment (μ_B/Mn)	Gap (eV)
NM	0.0	0.0	-
FM	-289.06	1.89	-
G-AFM	-544.07	3.21	0.31
C-AFM	-318.77	3.17	0.24

At ambient pressure, the optimized lattice constants for LaMnAsO are $a = 4.003$ Å and $c = 8.816$ Å, which is about 2.6% smaller than the experimental value [16, 17]. Using the optimized lattice constants and the numerical internal coordinates, several magnetic orders have been calculated to determine the ground state. The numerical results are summarized in Table. 1. In excellent agreement with the neutron scattering experiments [5, 16], the G-type AFM state has the lowest energy. At the same time, the experimental local moments of ~ 3.34 μ_B [17] could be well captured by the present GGA calculations, in which $m_{Mn} \sim 3.21$ μ_B. The notable reduced moment suggests an itinerant character and strong spin fluctuations of the AFM ground state, and could be regarded an a primary factor of metallization by the external pressure. The spin-polarized atom-projected density of states of the G-type AFM state is also plotted in Fig.

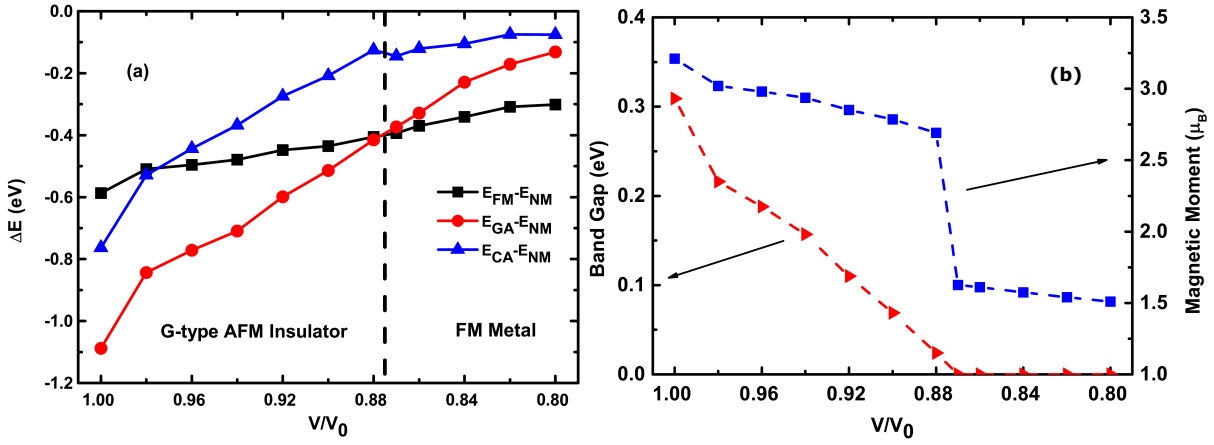

Figure 3. (Color online) (a) Total energy differences of FM (black line), G-type AFM (red line) and C-type AFM (blue line) states with respect to NM state over the volume ratio form 1.0 to 0.8 GPa. (b) The GGA band gap and magnetic moment are plotted as functions of volume ratio.

1 (b). While an intrinsic insulating behaviour is clearly shown by a band gap of ~ 0.31 eV at the Fermi level, another important feature of LaMnAsO compound is the relatively high PDOS near the bottom of conducting band, mostly from the Mn's $3d$ orbital. This suggests a possibility of a Stoner ferromagnetic instability against G-type AFM state provided that the G-type AFM gap is closed by the external pressure.

Using the above structural optimization procedure, we firstly show that LaMnAsO holds the expected tetragonal structure over the range of the volume ratio $\nu = \mathrm{V/V_0}$ from 1.0 to 0.8, where $\mathrm{V_0}$ is the volume at ambient pressure. The calculated variation of the a and c lattice parameters and the ratio c/a are shown in Fig. 2 (a) and (b), respectively. While the lattice parameters a and c decrease monotonically with the decrease in volume, there exits a distinct change of lattice parameters close to the ratio $\mathrm{V/V_0} \sim 0.87$, accompanied by a significant reduction in the ratio c/a. This means that the lattice parameter a becomes less compressible at high pressures, whereas the compressibility of the lattice parameter c shows a slight increase. The pressure intensity of different volume was quantified by using Birch-Murnaghan equation of state, and the numerical result is shown in the insert of Fig. 2 (b).

To study the relative stability of G-type AFM state against other possible magnetic state as increasing pressure, we perform numerical simulations on the three possible spin configurations (G-type AFM, C-type AFM, and FM) and the nonmagnetic (NM) state. Fig. 3 (a) displays the stabilization energies of these possible spin configurations relative to the NM state as a function of $\mathrm{V/V_0}$. Obviously, the G-AFM phase exhibits the lowest energy under the low pressure, but the total energy difference between the G-type AFM and FM state decreases with the decrease in volume. At the critical value of $\mathrm{V/V_0} \sim 0.87$, amounting to a pressure value $\mathrm{P}_c \sim 18$ GPa, a magnetic transition from the G-type AFM to FM state occurs, and additional decrease in volume further stabilizes the FM phase. The relationships among the volume $\mathrm{V/V_0}$, band gap and local Mn moment are shown in Fig. 3 (b). When the volume reaches to the critical value $\mathrm{V}_c \sim 0.87\mathrm{V_0}$, the bulk energy gap is closed, indicating that an insulator-to-metal (I-M) conversion happens along with the G-type AFM to FM transition occurring simultaneously. It is worthwhile to point out that the calculated V_c (or P_c) value likely represents a lower bound of the volume (or pressure) where the phase transitions occur, since the GGA method usually underestimate the band gap. In addition, while the substantial spin polarization of the G-type AFM state could be diminished by the decrease in volume, a high-spin to low-spin moment collapse rightly when

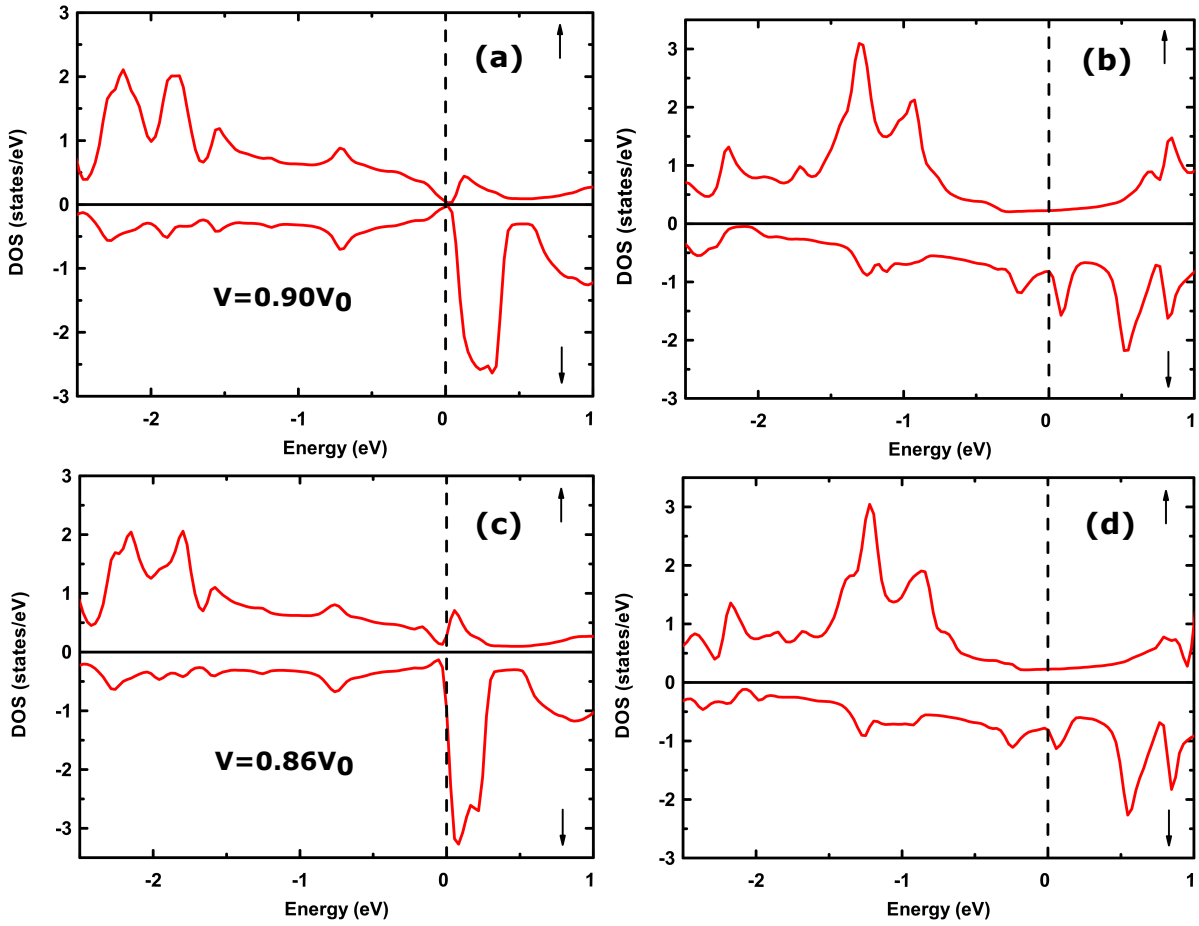

Figure 4. (Color online) Spin-polarized DOS of Mn at $V/V_0 = 0.9$ (a, b) and at $V/V_0 = 0.86$ (c, d) for G-type AFM (a, c) and FM (b, d) states, respectively.

the G-type AFM to FM transition comes at the critical V_c, as seen in Fig. 3 (b). Physically that is correlated with the Hund's metal nature of the FM state, in which the itineration of electrons enforces the spin up and down symmetrical distribution of electrons within the Mn $3d$ shell, but the Hund's rule coupling is unnecessarily reduced to zero under the present pressure, yielding a rapid reduction of the local moment down to the finite value $\sim 1.63\ \mu_B$.

To further illustrate the profound magnetic and electronic transition of the pressured LaMnAsO, the spin-polarized density of states of Mn cation are plotted in Fig. 4 for both of the G-type AFM and FM states at $V/V_0 = 0.90$ and $V/V_0 = 0.86$. Despite a little increase of the density of states near the bottom of conducting band, one could clearly notice that the overall profile of density of states for both of the G-type AFM and FM cases do not change much as was previously appreciated. When the external pressure is higher than the critical value P_c, the band gap of the G-type AFM state has been closed and the Fermi level is shifted to the high density of states of the conducting band. Hence the Stoner instability make the system metallic FM ordering according to optimizing the kinetic energy of the polarized state and suppressing the density of states of the G-type AFM state at the Fermi level.

4. Summary

In summary, we have investigated the effect of hydrostatic pressure on the G-type AFM insulator LaMnAsO using a full potential linearized augmented plane-wave method. The I-M transition accompanied by the emergence of FM state is predicted at the critical pressure $P_c \sim 18.0$ GPa. Meanwhile a high-spin to low-spin moment transition is also revealed when the I-M transition occurs. It is the hydrostatic pressure that drives the collapse of the G-type AFM gap of LaMnAsO, and then the high density of state around Fermi level stabilizes the metallic FM phase due to the Stoner instability. Since the pressure modulation drives the insulator-metal transition, these results open up the possibility of two-state device applications based the oxypnictide LaMnAsO compound.

5. Acknowledgments

The author (H.B.) would like to thank LiangJian Zou for valuable suggestions, discussions and carefully reading of the manuscript. The work was financially supported by the National Sciences Foundation of China under Grant Nos. 11574315 and 21403001.

References

[1] Kamihara Y, Watanabe T, Hirano M, and Hosono H 2008 *J. Am. Chem. Soc.* **130** 3296
[2] Takahashi H, Igawa K, Arii K, Kamihara Y, Hirano M, and Hosono H 2008 *Nature* (London) **453** 3296
[3] Chen X H, Wu T, Wu G, Liu R H, Chen H, and Feng D L 2008 *Nature* (London) **453** 761
[4] Marcinkova A, Hansen T C, Curfs C, Margadonna S, and Bos J W G 2010 *Phys. Rev. B* **82** 174438
[5] Emery N, Wildman E J, Skakle J M S, Giriat G, Smith, R I and Mclaughlin A C 2010 *Chem. Commun.* **46** 6777
[6] Tsukamoto Y, Okamoto Y, Matsuhira K, Whangbo M H, and Hiroi Z 2011 *J. Phys. Soc. Jpn.* **80** 094708
[7] Wildman E J, Skakle J M S, Emery N, and Mclaughlin A C 2012 *J. Am. Chem. Soc.* **134** 8766
[8] Yanagi H, Kawamura R, Kamiya T, Kamihara Y, Hirano M, Nakamura T, Osawa H, and Hosono H 2008 *Phys. Rev. B* **77** 224431
[9] Ohta H and Yoshimura K 2009 *Phys. Rev. B* **80** 18409
[10] McGuire M A, Gout D J, Garlea V O, Sefat A S, Sales B C, and Mandrus D 2010 *Phys. Rev. B* **81** 104405
[11] Marcinkova A, Grist D A M, Margiolaki I, Hansen T C, Margadonna S , and Bos J W G 2010 *Phys. Rev. B* **81** 065511
[12] Li Z, Chen G, Dong J, Li G, Hu W, Wu D, Su S, Zheng P, Xiang T, Wang N, and Luo J 2008 *Phys. Rev. B* **78** 060505(R)
[13] Matsuishi S, Nakamura A, Muraba Y, and Hosono H 2012 *Supercond. Sci. Technol.* **25** 084017
[14] Luo Y, Han H, Tan H, Lin X, Li Y, Jiang S, Feng C, Dai J, Cao G, Xu Z, and Li S 2011 *J. Phys.: Condens. Matter* **23** 175701
[15] McGuire M A, Garlea V O, May A F, and Sales B C 2014 *Phys. Rev. B* **90** 014425
[16] Kayanuma M A, Hiramatsu V O, Kamiya A F, Hirano A F and Hosono B C 2009 *J. Appl. Phys.* **105** 073903
[17] Emery N, Wildman E J, Skakle J M S, Mclaughlin A C, Smith R I, and Fitch A N 2011 *Phys. Rev. B* **83** 14429
[18] Cruz C, Huang Q, Lynn J M, Li J Y, Ratcliff W, Zarestky J L, Mook H A, Chen G F, Luo J L, Wang N L, and Dai P C 2008 *Nature* **453** 899
[19] Xu G, Ming W, Yao Y, Dai X, Zhang S C, and Fang Z 2008 *Europhys. Lett.* **82** 67002
[20] Sun Y, Bao J, Feng C, Xu Z, and Cao G 2012 *Europhys. Lett.* **98** 17009
[21] Hanna T, Matsuishi S, Kodama K, Otomo T, Shamoto S, and Hosono H 2013 *Phys. Rev. B* **87** 020401(R)
[22] Blaha P, Schwarz K, Madsen G K H, Kvasnicka D, and Luitz J, 2001 *WIEN2K, An Augmented Plane Wave+ Local Orbitals Program for Calculating Crystal Properties* (Karlheinz Schwarz, Technische Universitat Wien, Austria)
[23] Perdew J, Burke K, and Ernzerhof M 1996 *Phys. Rev. Lett.* **77** 3865